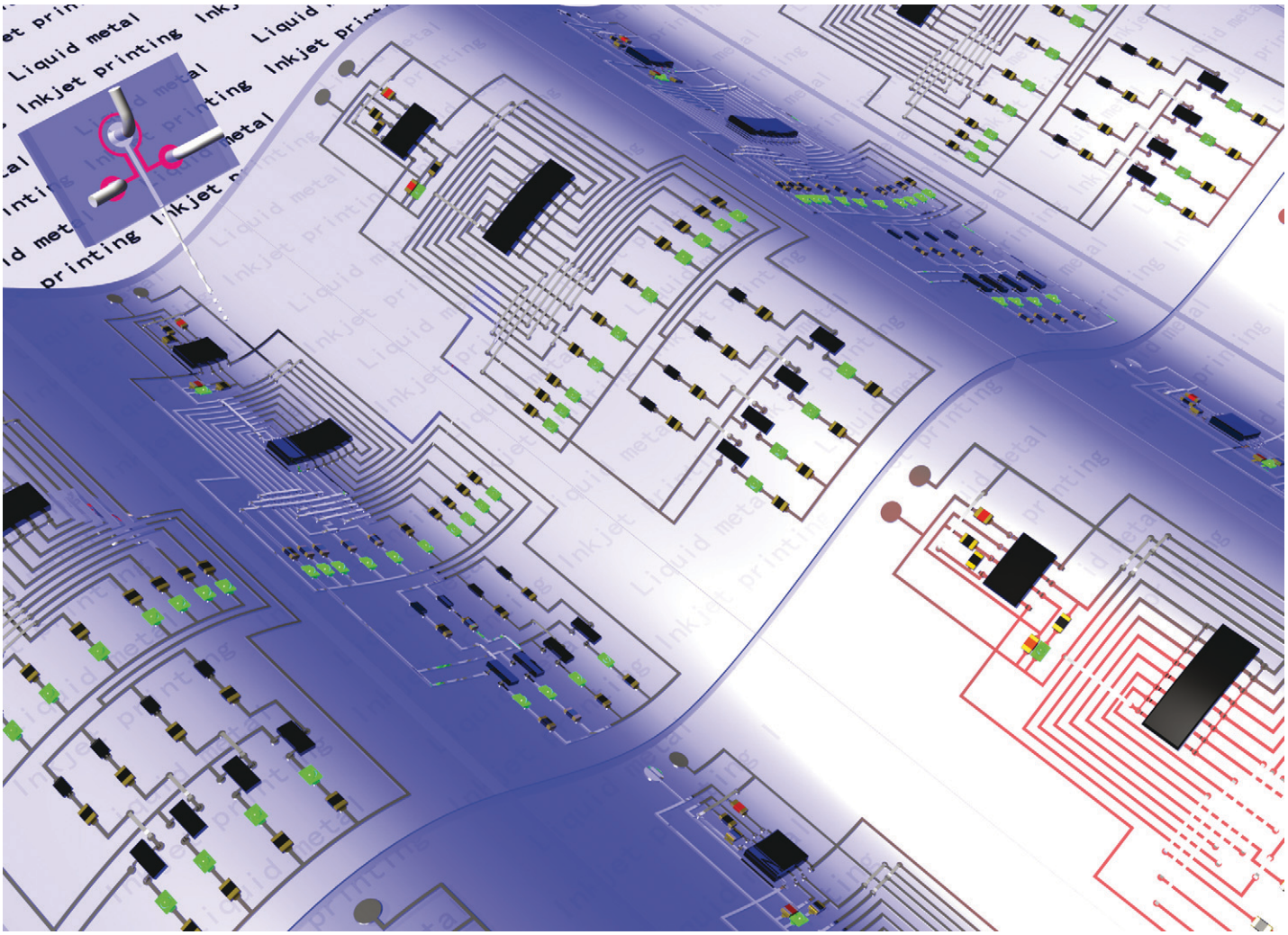


**Featuring work from the MEMS and Nanotechnology Laboratory in the School of Mechanical Engineering at Chonnam National University, Gwangju, South Korea.**

Title: A galinstan-based inkjet printing system for highly stretchable electronics with self-healing capability

We present a Galinstan-based inkjet printing system to realize stretchable electronics with the capability of extremely large deformation and self-healing. Experimental results reveal that the proposed idea has tremendous potential for next generation electronics.

## As featured in:

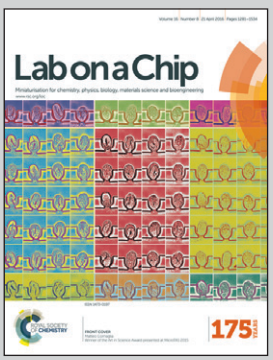


See Dong-Weon Lee *et al. Lab Chip*, 2016, **16**, 1366.

ROYAL SOCIETY OF CHEMISTRY

www.rsc.org/loc

Registered charity number: 207890

Lab on a Chip

PAPER

# A galinstan-based inkjet printing system for highly stretchable electronics with self-healing capability†

Guangyong Li, Xuan Wu and Dong-Weon Lee*

Cite this: *Lab Chip*, 2016, **16**, 1366

Received 12th January 2016,
Accepted 4th March 2016

DOI: 10.1039/c6lc00046k

www.rsc.org/loc

We report a galinstan-based inkjet printing system to realize highly stretchable electronics with self-healing capability. The printing head made of polydimethylsiloxane (PDMS) consists of a main microfluidic channel and a coplanar channel. The main channel containing the oxidized galinstan is surrounded by the coplanar channel, which is filled with HCl. The HCl vapor effectively permeates the channel wall due to the high gas permeability of PDMS. The oxide skin of galinstan is consistently removed by chemical reaction with the HCl vapor. This allows one to maintain galinstan in a true liquid phase in the main channel. After the fabrication of the printing head with PDMS, the sizes of droplets ejected from the printing head with various flow rates have been characterized. The fabricated inkjet printing system is also utilized to generate complex galinstan patterns on various substrates. An LED-integrated circuit with self-healing capability shows excellent electrical and mechanical performance even after it is twisted more than 180° or stretched up to ~60% more than 2000 times. The experimental results reveal that the proposed system has tremendous potential for stretchable electronic applications in the future.

## Introduction

The use of stretchable electronics is highly preferred for designing flexible electronic devices due to their unique stretchability and improved mechanical robustness.[1–8] Recently, various fabrication techniques have been developed to realize stretchable electrical interconnectors, such as stencil mask-based printing,[5,6] direct writing,[9–14] atomized spraying,[8,15,16] injection,[17–21] masked deposition,[22] liquid metal plating,[23] and inkjet printing.[24] Unlike other fabrication techniques, inkjet printing is a non-contact type of fabrication method, which can enhance the mass production rate.

Galinstan is a widely used ink for patterning stretchable electronics.[25,26] It is a commercially available (Geratherm Medical AG, Germany) non-toxic liquid metal alloy with the composition Ga–In–Sn (68.5%, 21.5% and 10% by weight, respectively). It has excellent physical properties such as low melting point, low electrical resistivity, high boiling point, high thermal conductivity, and ultralow vapor pressure. Moreover, it does not require dispersion in a solvent compared with conductive polymer and silver nanoparticle inks. Even after being printed, this liquid metal maintains its fluidic performance with high 3D conformability following arbitrary mechanical deformation of the substrate.

*MEMS and Nanotechnology Laboratory, School of Mechanical Engineering, Chonnam National University, Gwangju, 61186, South Korea.*
*E-mail: mems@chonnam.ac.kr; Fax: +82 62 5300337; Tel: +82 62 5301669*

† Electronic supplementary information (ESI) available. See DOI: 10.1039/c6lc00046k

However, the critical issue in inkjet printing is clogging of the inkjet nozzle. This is because galinstan is easily oxidized in an air environment and behaves more like a gel rather than a true liquid. The oxide layer of galinstan behaves like a solid, which stacks in the nozzle and causes clogging. Nevertheless, galinstan processed with the coplanar channel-based reduction technology (CCRT) behaves like a true liquid phase in an open atmosphere, as discussed in our previous works.[27,28] Even when the liquid metal is oxidized, it still exhibits a non-wetting behavior in surface-modified polydimethylsiloxane (PDMS) channels.[29]

In this study, based on the reduction technology, a gas-permeable PDMS-based coplanar microfluidic channel structure is introduced to fabricate the head of a galinstan-based inkjet printer. Galinstan in the nozzle channel can remain in the true liquid phase when its surrounding coplanar channel is filled with HCl solution. After studying the characteristics of the proposed nozzle, a galinstan-based inkjet printing system is developed to realize various complex liquid metal patterns on a stretchable substrate. The effectiveness and reliability of the galinstan-based inkjet printing system are evaluated with an LED-integrated liquid metal circuit under various conditions such as bending, twisting, and stretching.

## Basic theory

### Reduction of oxidized galinstan

Although galinstan has been investigated for many electronic device applications, the superfast surface oxidation of the liquid metal restricts its wide applicability. Actually, the oxide


This journal is © The Royal Society of Chemistry 2016

layer on the surface of galinstan is an elastic solid and has a yield stress.[30–32] In addition, its viscous nature largely originates from gallium oxide ($Ga_2O_3$), which is sufficiently sticky to prevent easy movement. As shown in Fig. S1(a1 and a2) of the ESI,† the oxidized galinstan easily adheres on the PDMS channel wall and forms irregular shapes, which can clog the microfluidic channel. However, galinstan can exhibit the true liquid phase when the coplanar microfluidic channels are filled with 37 wt% HCl solution as shown in Fig. S1(b1) of the ESI.† Due to the excellent permeability of PDMS, HCl vapor can permeate through the PDMS wall between the two channels (sub-channel and main channel) and reduce gallium oxide, as illustrated in Fig. S1(b2) of the ESI.† The thickness of the PDMS wall is also one of the important parameters that determine the diffusion time of HCl, and this has been optimized in a previous work.[27] Considering the safety issues associated with using HCl solution (which is generally 37 wt%), it was further diluted to 30, 23, and 16 wt%. In such low-concentration HCl solutions, increasing the operating temperature of the nozzle was found to be effective in ensuring successful diffusion of the HCl vapor across the PDMS channel. In order to prevent leakage of the HCl vapor into the air, Parlyene (PPX) was coated on both surfaces using a chemical vapor deposition technique. Aside from the coplanar channel-based reduction technology (CCRT), the oxidation surface of galinstan can also be removed by using NaOH (sodium hydroxide) solution, and the processed liquid metal droplet can be easily controlled with the applied voltage based on the electrochemistry theory.[33] Although the liquid metal droplet moves freely, it must be immersed in NaOH (sodium hydroxide) solution. For the CCRT, the liquid metal droplet needn't be surrounded by HCl solution and only need contact with HCl vapor.

### Inkjet theory and simulation

The inkjet printing method is a promising technique with great potential for flexible electronics. There are two main technologies in contemporary inkjet printers. One of them is continuous ink jet (CIJ) and the other is drop-on-demand (DOD), which can be sub-divided into thermal DOD and piezoelectric DOD. For thermal DOD, a current pulse is passed through the heater to cause rapid vaporization of the ink in the chamber, thereby propelling a droplet of ink onto the target. For piezoelectric DOD, when a voltage is applied, the piezoelectric material changes shape, generating a pressure pulse in the fluid, which forces a droplet of ink from the nozzle. In our study, the galinstan droplet is generated from the nozzle based on the principle of Rayleigh instability.[34]

The liquid ejected from the nozzle with a lower flow rate forms a pendant droplet (a leaking faucet), which is characterized by a quasi-static balance between surface tension and inertial forces.[35–38] The mechanism of droplet formation in this phenomenon is widely described as "dripping." When the liquid flow rate is increased such that the Weber number (We) is larger than 4, a liquid jet stream is generated at the end of the nozzle, as shown in Fig. 1.[39] The relationship between liquid velocity and the We can be expressed using the following equation:[39]

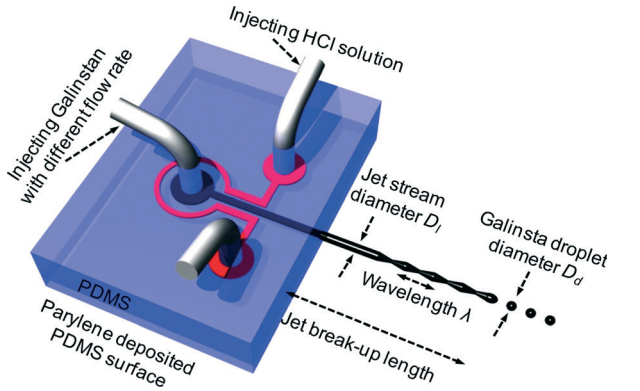


Fig. 1 Conceptual schematic of galinstan droplet generation based on the principle of Rayleigh instability.

$$\mathrm{We} = \frac{\rho_l D_l v^2}{2\gamma} \quad (1)$$

where $D_l$ is the diameter of the jet stream, $\rho_l$ is the liquid density, $v$ represents the velocity of the liquid, and $\gamma$ is the surface tension of the liquid. Due to Rayleigh instability, the jet stream spontaneously breaks up into small droplets to minimize its surface energy.[34] A small sinusoidal perturbation with wavelength $\lambda$ can grow the disturbance sinusoidally with space and exponentially with time, which is described as the classical Rayleigh–Plateau instability:[34]

$$R(z,t) = \frac{D_l}{2} + \delta e^{\omega(t-t_0)} \cos\left(\frac{2\pi z}{\lambda}\right) \quad (2)$$

where $z$ is the axial position on the jet stream, $\omega$ is the growth rate of the perturbation amplitude, and $\delta$ is the amplitude of the perturbation at $t = t_0$. When the flow rate is fixed, the jet breakup length $L$ is determined by the growth rate which is affected by the size of the nozzle, and the density and surface tension of the liquid. In addition, the approximate volume of the generated liquid droplet is calculated by using the formula $\lambda\pi D_l^2/4$, from which we can determine the diameter $D_d$ of the galinstan droplet.[40]

COMSOL Multiphysics was employed for better understanding of the dynamic behavior of galinstan inkjet. Fig. 2 shows the simulation results of the galinstan droplet ejected from the inkjet nozzle with different flow rates after 0.5 ms. For low flow rates ($\leq$0.1 mL min$^{-1}$), the inkjet nozzle (cross-section size: 40 μm width × 10 μm height) only generates galinstan droplets at the end of the nozzle device, as shown in Fig. 2(a). The volume of the galinstan increases with time. For high flow rates ($\geq$0.2 mL min$^{-1}$), the galinstan is ejected from the nozzle and forms a jet stream. Subsequently, the jet stream breaks up into several small galinstan droplets due to Rayleigh instability, as shown in Fig. 2(b–e).[34] If there is no HCl vapor which effectively removes the oxide layer of galinstan, the liquid metal ejected from the nozzle can

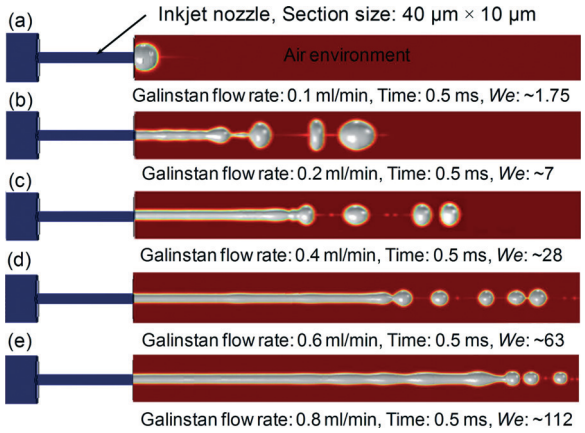


**Fig. 2** Inkjet simulation results with flow rates of (a) 0.1 mL $min^{-1}$, (b) 0.2 mL $min^{-1}$, (c) 0.4 mL $min^{-1}$, (d) 0.6 mL $min^{-1}$, and (e) 0.8 mL $min^{-1}$.

maintain a stable fiber-shape in an air environment, which has been discussed by Dickey's group.[12] Apart from obtaining a better understanding of the ejection of galinstan inkjet, the simulation can also be used to predict the optimal design of a nozzle. The diameters of the jet stream and galinstan droplet are primarily determined by the section size of the nozzle. In order to obtain a smaller galinstan droplet and a high-resolution galinstan line, three inkjet nozzles with different sizes (cross-section size: 40 μm width × 10 μm height, 20 μm width × 10 μm height, 10 μm width × 10 μm height) were fabricated and studied in the next step.

## Fabrication of galinstan-based inkjet nozzle

The galinstan-based inkjet nozzle was fabricated using conventional micro-molding technology. The fabrication steps are described in Fig. 3(a). The mold of the inkjet nozzle with a coplanar microfluidic channel was fabricated from a SU-8 2050 photoresist (PR) on a silicon wafer. PDMS solution was coated on the inkjet nozzle mold using the standard rapid prototyping method. After curing, the top PDMS layer was gently peeled off from the mold. The PDMS layer (thickness: 3 mm) contains an inkjet nozzle channel which was surrounded by a coplanar channel (cross-section size: 250 μm width × 10 μm height). Here, we chose three different sizes of the nozzle channel (cross-section size: 40 μm width × 10 μm height, 20 μm width × 10 μm height, 10 μm width × 10 μm height) to study the dynamic behavior of galinstan inkjet. The cross-section size of the internal PDMS wall between the two channels is 200 μm width × 10 μm height. The designed channels contain 3 ports (diameter: 2.4 mm) that were used to inject galinstan as well as HCl solution. The PDMS channel layer and the flat PDMS layer (as foundation base, thickness: 2 mm) were bonded together after oxygen plasma treatment. After bonding, the excess part of the channel was cut to complete the nozzle formation. Finally, 1 μm thick Parylene (PPX) coating was deposited on the surface of the nozzle device to prevent HCl evaporation from the PDMS channel, as shown in Fig. 3(b). As shown in Fig. 3(a6), first, HCl solution was injected into the coplanar channel. Subsequently, galinstan was injected into the nozzle channel to form the true liquid droplet.

## Generation and jetting of galinstan droplet

In order to validate the effectiveness of the reduction technique, the behavior of galinstan in the nozzle is studied when the coplanar channel is filled with and without 37 wt% HCl solution as shown in Fig. S2.† The cross-section size of the fabricated nozzle channel is 40 μm width × 10 μm height. As shown in Fig. S2(a) of the ESI,† an air pressure of ~155 kPa is required to inject the galinstan into the narrow nozzle channel from the wide port when the coplanar channel is empty. Also, the galinstan cannot move further even when the air pressure is increased to ~200 kPa. This is due to the fact that the galinstan in the channel is oxidized and sticks to the inner channel surface. On the other hand, an air pressure of only ~70 kPa is required for injection when the

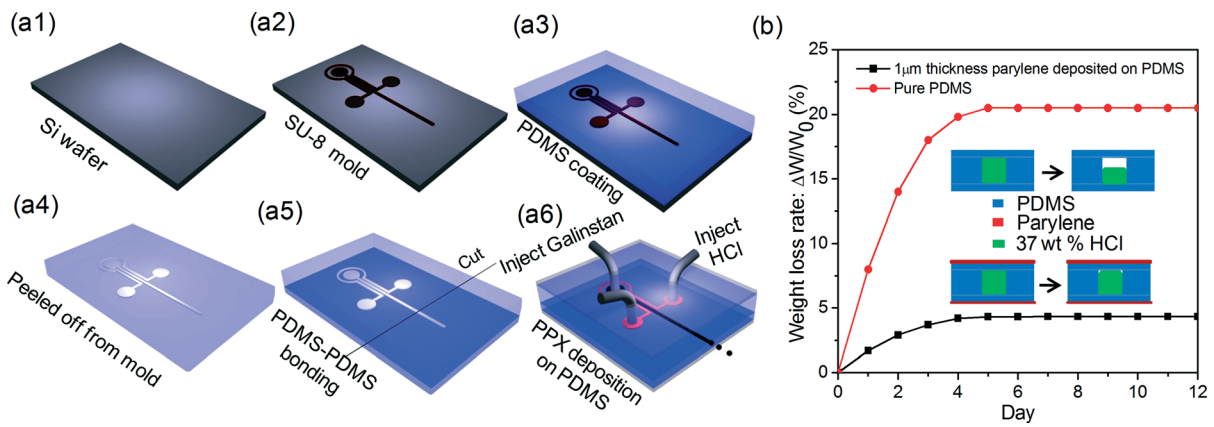


**Fig. 3** Fabrication sequence of a galinstan-based inkjet nozzle: (a1) Si wafer, (a2) SU-8 PR mold on Si wafer, (a3) PDMS coating, (a4) PDMS peeled off from the mold, (a5) PDMS–PDMS bonding and cutting, and (a6) injection of galinstan into an inkjet nozzle channel surrounded by another coplanar channel filled with HCl solution. (b) Prevention of HCl evaporation by using Parylene coating.

 This journal is © The Royal Society of Chemistry 2016

coplanar channel is filled with 37 wt% HCl solution, as shown in Fig. S2(b) of the ESI.† Moreover, the galinstan can continue flowing without any further increment in air pressure.

As discussed before, at lower flow rates, the inkjet nozzle only generates one galinstan droplet at the end of the nozzle and, at higher flow rates, the galinstan ejected from the nozzle forms a jet stream, which breaks up into several small galinstan droplets subsequently. Thus, the minimum flow rate of the galinstan should be sufficient for obtaining a suitable Weber number, which enables the formation of a jet stream and droplets. The experimental and simulation results for the minimum flow rate *versus* nozzle width are shown in Fig. S3 of the ESI.† For the nozzle with a cross-section size of 40 μm width × 10 μm height, the minimum flow rate, as obtained experimentally, is ~0.19 ml $min^{-1}$, which is slightly higher than the simulation result. This is due to the use of an elastomer material (PDMS) as the nozzle. With a higher flow rate, deformation of the nozzle shape is observed and the cross-section size is increased slightly due to higher internal pressure. However, in simulation, the material of the nozzle is considered to be ideal and non-deformable and therefore the simulation result is larger than the real value. As expected, the minimum flow rate required for droplet formation decreases with reducing nozzle width, as shown in Fig. S3 of the ESI.†

Next, the behavior of galinstan ejected from the various-size nozzles with different flow rates is characterized as shown in Fig. 4. For the nozzle with a cross-section of 40 μm width × 10 μm height, the average diameter of the galinstan droplet is ~78 μm with a flow rate of 0.2 ml $min^{-1}$, as shown in Fig. 4(a and c). The distribution of the galinstan droplet diameter is analyzed as shown in Fig. 4(b). The diameter of the galinstan droplet ranges from ~55 μm to ~93 μm, which matches with the simulation result as shown in Fig. 2. By varying the flow rates, droplets with smaller sizes are created. The average diameter of the droplet decreases with the increase in flow rate as shown in Fig. 4(c). A higher flow rate implies a higher jetting velocity, which is the flow rate divided by the cross-sectional area of the nozzle. An increase in the jetting velocity can subsequently reduce the wavelength, $\lambda$. With the decrease in wavelength, the probability of forming smaller droplets is increased.[41] With a fixed flow rate, the galinstan droplet size is determined by the nozzle size. As Fig. 4(c) shows, galinstan droplets with a diameter of ~10 μm (volume of ~0.5 femtoliter) can be generated when the cross-section of the nozzle is 10 μm width × 10 μm height with a flow rate of 0.8 ml $min^{-1}$. Micro-scale (hundreds of μm to several tens of μm) galinstan droplets can also be produced by using flow-focus devices proposed by Thelen *etc.*, which can be applied to electrodes, switches, and optical gratings.[42–45] However, those techniques still need to be improved to make desired complex patterns on elastic substrates for flexible electronic applications. Here, we generated an array of micro-scale galinstan droplets and printed it on a PDMS substrate to realize stretchable electronics.

## Galinstan-based inkjet printing

After characterizing the behavior of galinstan jetting, the printing system (described in Fig. S4 of the ESI†) was used for galinstan-based inkjet printing. Due to the continuous chemical reaction between the oxide skin and HCl vapor, the

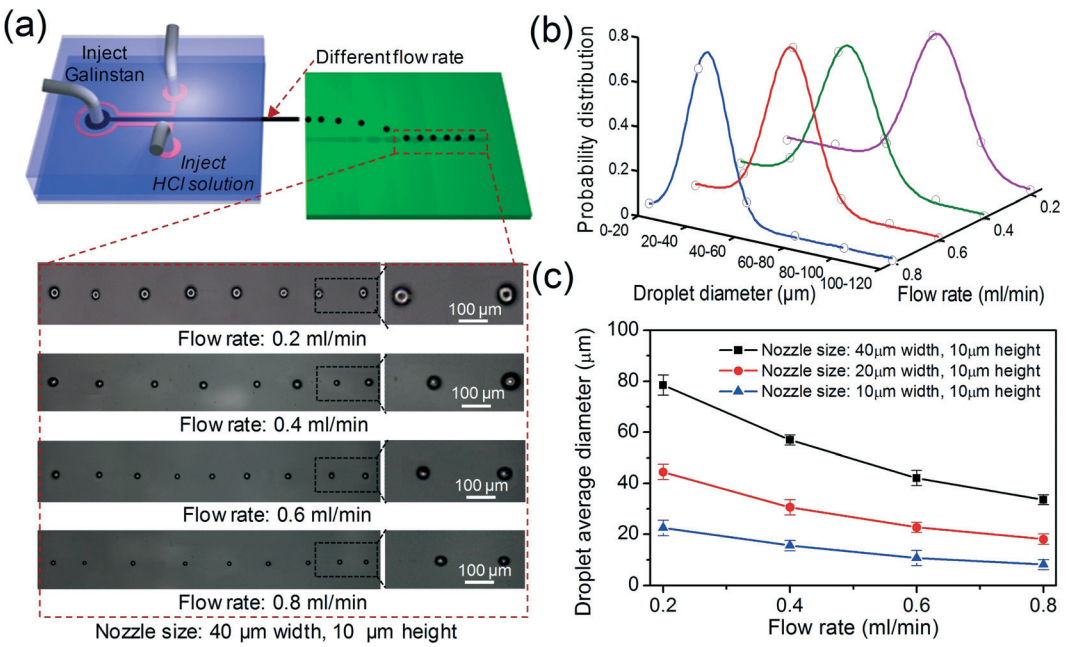


**Fig. 4** Characterization of the galinstan droplet ejected from the inkjet nozzle. (a) Galinstan droplet ejected from the fabricated nozzle (40 μm width, 10 μm height) with different flow rates, (b) probability distribution of the diameter of the galinstan droplet ejected from the nozzle (40 μm width, 10 μm height) with different flow rates, and (c) average diameter of the galinstan droplet ejected from different-size nozzles with different flow rates.

galinstan droplets ejected from the nozzle maintain a true liquid phase for a split second. However, it seems that the droplets start to reform the oxide skin during the transfer from the nozzle to a substrate. This phenomenon is confirmed using a simple experiment with a syringe as shown in SV. 1 and 2 of the ESI.† The oxidation time depends on the volume of HCl vapor at the surface of the galinstan droplets. The distance between the printing head and the substrate is about 20 mm. The galinstan flow rate was controlled using a LabVIEW controlled syringe pump. The movement and velocity of the *X–Y–Z* stage were controlled by an ESP 300 controller. It is easy to envisage that the resolution of the galinstan pattern can be affected by the galinstan flow rate and the velocity of the *X–Y–Z* stage. With higher velocity of the *X–Y–Z* stage, a galinstan line with smaller width can be formed. Thus, the relationship between the flow rate and the velocity is studied as shown in Fig. S5 of the ESI.† As demonstrated in Fig. S5(a), the jet stream and droplets ejected from the nozzle fall on the substrate and form a galinstan line when the *X–Y–Z* stage is moved at a velocity of 10 cm $s^{-1}$. The average width of the galinstan line increases with the increase in flow rate. The reason is that a higher flow rate results in a higher jetting velocity and as a result, over the same time period and distance, a larger volume of galinstan is transferred from the galinstan reservoir to the substrate surface. When the flow rate is constant, the width of the galinstan line decreases with an increase in the velocity of the *X–Y–Z* stage, as shown in Fig. S5(b) of the ESI.† A galinstan line with a width of ~100 μm can be obtained by using the nozzle (40 μm width) with a flow rate of 0.2 ml $min^{-1}$ and a stage velocity of 10 cm $s^{-1}$. A smaller width galinstan line can be obtained by further increasing the velocity of the *X–Y–Z* stage or reducing the nozzle size.

In order to evaluate the galinstan-based inkjet printing, various complex galinstan patterns are formed on different substrates, as shown in Fig. 5. As observed from Fig. 5(a), the galinstan line is formed on normal A4 paper. The 40 μm-width nozzle was used here with a higher flow rate (0.6 ml $min^{-1}$) and a higher moving velocity of the paper (~0.6 m $s^{-1}$). The occasional non-uniformity of the galinstan line is due to the probability distribution of the size of the jetting droplet. Although the average diameter of the galinstan droplet is ~48 μm, larger size droplets are occasionally generated and form the "bulge" shape, which is due to Rayleigh instability.[34] As shown in Fig. 5(b–d), galinstan lines with straight, sawtooth, and serpentine shapes are formed on the PDMS. The shape of the galinstan pattern is determined by controlling the *X–Y–Z* stage with an in-house developed program. Here, a flow rate of 0.2 ml $min^{-1}$ and an *X–Y–Z* stage velocity of 10 cm $s^{-1}$ are used. After the formation of a complex galinstan pattern on PDMS, the patterned substrate was coated with standard PDMS solution (base/agent ratio, 10 : 1) and cured at 60 °C for 2 h, as shown in Fig. 5(e–h). The galinstan patterns that emerged on the PDMS exhibit excellent mechanical performance after deformation such as bending, twisting, and stretching.

## Application to stretchable electronics

To explore the potential of galinstan-based inkjet printing in electronic applications, stretchable galinstan wires with various shapes were fabricated. Fig. 6(a) shows the change in resistance of the galinstan wires with various shapes (straight, sawtooth, and serpentine) with stretching. Compared with other shapes, the serpentine-shaped galinstan wire exhibits more stable electrical properties even after being stretched to 80%. As shown in Fig. 6(b), the resistance of the serpentine-shaped galinstan wire shows only a slight change even after twisting and bending to 180°. Therefore, any influence on the electrical performance as a result of deformation is almost negligible. After patterning the serpentine-shaped galinstan wire on a PDMS substrate, an LED is integrated on its surface. Finally, PDMS solution is covered on the sample integrated with LEDs and cured to firmly fix the LEDs in the

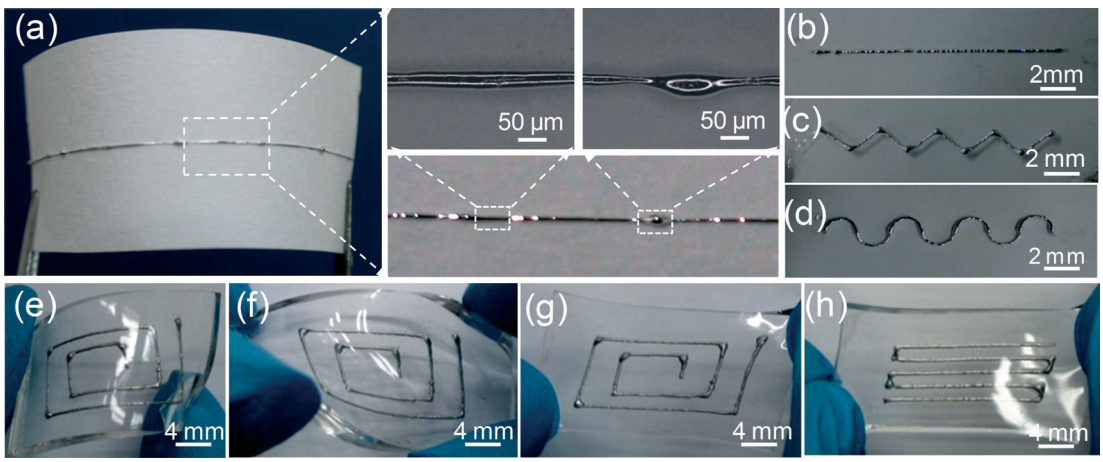


**Fig. 5** Complex galinstan patterns formed on various substrates by galinstan-based inkjet printing. (a) Galinstan line formed on normal A4 paper. (b–d) Galinstan lines with straight, sawtooth, and serpentine shapes formed on PDMS. (e–h) Deformation (bending, twisting, and stretching) of the galinstan pattern with a dual rectangular and square spiral shape emerged on the PDMS.

 This journal is © The Royal Society of Chemistry 2016

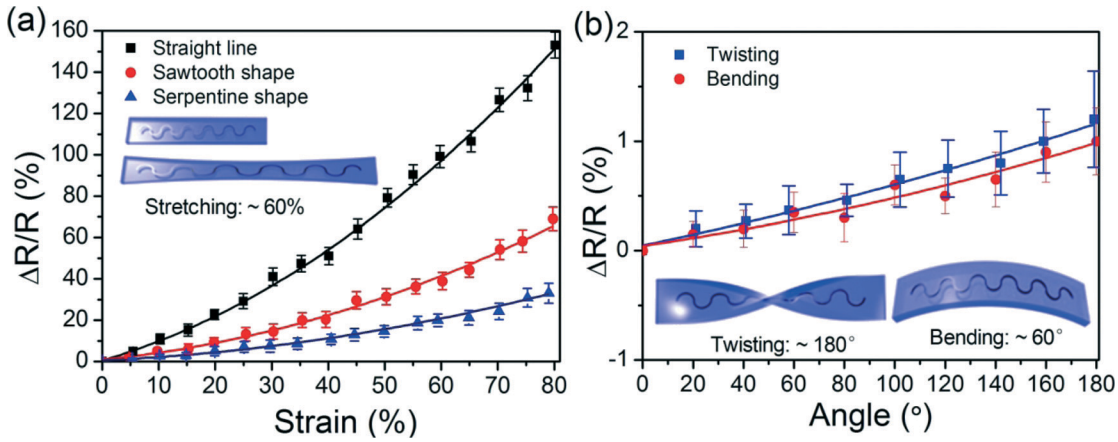


**Fig. 6** Electrical characterization of galinstan wires with various shapes. (a) Change in the resistance of the galinstan wire with applied strain and (b) change in the resistance of the galinstan wire (serpentine shape) with twisting and bending deformation.

PDMS film. Fig. 7(a–d) show a serpentine-shaped galinstan wire integrated with an LED. Stable performance is successfully maintained, even for an applied bend of 60°, a twist of 180°, or a strain of 60%. Fig. 7(e–f) shows the self-healing capability of the stretchable galinstan circuit. The stretchable circuit is severed with scissors and self-heals electrically under ambient conditions, which can also be used for tunable antennas.[46] No additional force is required for the reconnection of the electrically broken wire. Fig. 7(g) presents the *I–V* characteristics of the LED-integrated galinstan circuit, which displays stable performance with a degradation of less than 2% under various types of mechanical deformation (bending, twisting, stretching and cutting–reconnection). The LED-integrated galinstan circuit also shows excellent stable

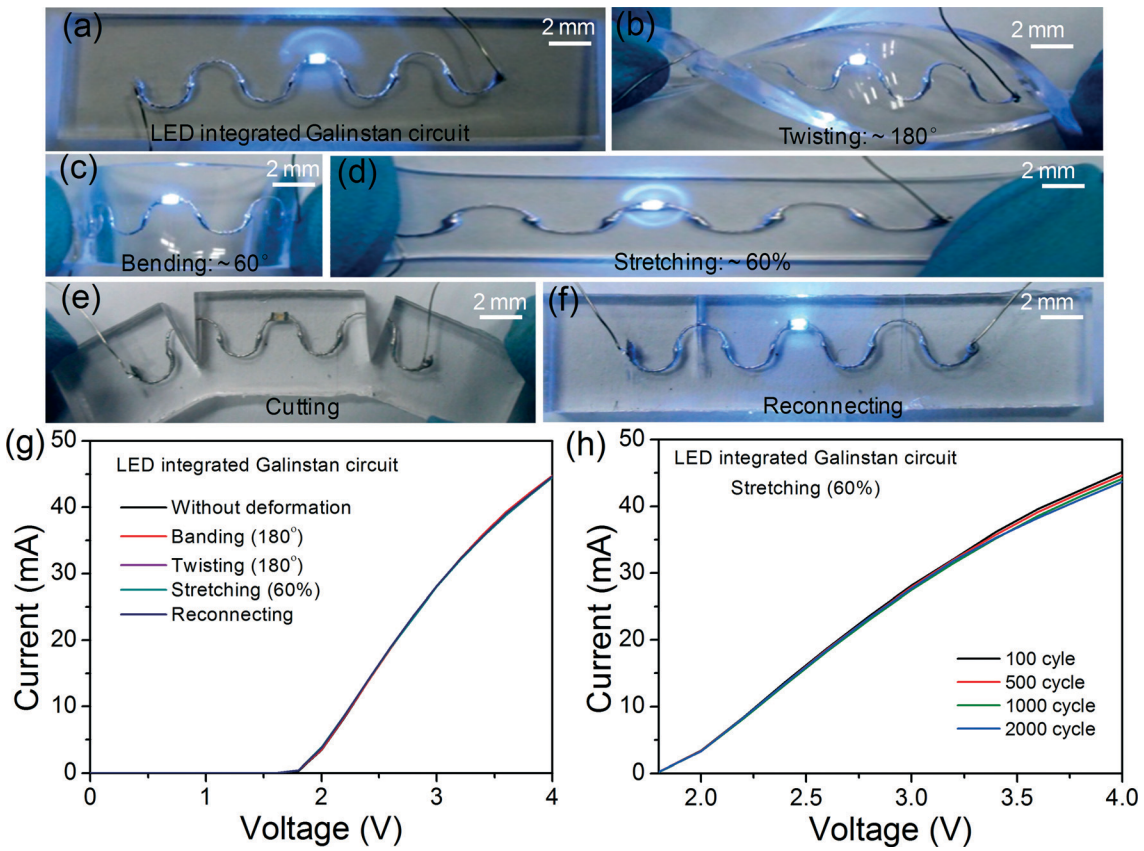


**Fig. 7** *I–V* characterization of an LED-integrated galinstan circuit. (a–d) LED-integrated galinstan circuit (serpentine shape) with an external power supply of 3 V (3D mechanical deformation). (e) Physical separation of the LED-integrated galinstan circuit with a blade. (f) Reconnection of the LED-integrated galinstan circuit. (g) *I–V* characteristics of the LED-integrated galinstan circuit under various types of mechanical deformation (bending, twisting, and stretching). (h) *I–V* curves of the LED-integrated galinstan circuit upon repeated stretching.

electrical performance even when stretching of the circuit with a strain of 60% is repeated 2000 times, as shown in Fig. 7(h).

## Conclusion

We present a novel approach for producing stretchable circuits by using a galinstan-based inkjet nozzle with a gas-permeable PDMS-based coplanar microfluidic channel structure. Galinstan in the nozzle maintains a true liquid phase when the coplanar microfluidic channel is filled with HCl solution. A galinstan droplet with a diameter of ~10 μm (volume of ~0.5 femtoliter) can be generated by using the proposed nozzle with a cross-section of 10 μm width × 10 μm height and a flow rate of 0.8 ml $min^{-1}$. The galinstan-based inkjet printing can produce various complex galinstan patterns with planar dimensions less than 50 μm without the requirement of an airbrush and a stencil mask. The results of the resistance change with deformation demonstrate that the serpentine-shaped galinstan wire exhibits the most stable electrical properties under 3D deformation. To further verify the feasibility of the galinstan-based inkjet printing, an LED-integrated galinstan circuit was fabricated and evaluated under various conditions such as bending, twisting, or stretching. The *I–V* characteristics reveal that the circuit exhibits stable electrical and mechanical properties, even after 2000 stretching (60%) cycles. However, the diversity of droplet diameter has a large influence on the quality and resolution of the liquid metal pattern (forming the "bulge" shape). Therefore, more efforts should be focused on how to achieve a more uniform size of the galinstan droplet in our future work. One method is to combine piezoelectric drop-on-demand or thermal drop-on-demand technology with the printing head. When a fixed current or voltage pulse is applied, the volume of the droplet could maintain a constant value. In this case, the diameter of the galinstan droplet ejected from the nozzle can be more uniform. We expect that further improvement of this technology will yield the ability to combine stretchable galinstan wires with multiple-functional electronic elements for the creation of novel electronic devices such as wearable electronic clothing, stretchable displays, skin sensors, and other advanced electronics.

## Acknowledgements

This study was supported by a grant from the Korean Health Technology R&D Project (HI13C1527), Ministry of Health & Welfare and the International Collaborative R&D Program through a KIAT grant funded by the MOTIE (N0000894), and the National Research Foundation of Korea grant funded by the government of Korea (no. 2015R1A2A2A05001405).

## References

1 D. M. Vogt, Y.-L. Park and R. J. Wood, *IEEE Sens. J.*, 2013, **13**, 4056–4064.
2 R. D. P. Wong, J. D. Posnerb and V. J. Santosa, *Sens. Actuators, A*, 2012, **179**, 62–69.
3 S. Cheng and Z. G. Wu, *Adv. Funct. Mater.*, 2011, **21**, 2282–2290.
4 B. M. Kubo, X. Li, C. Kim, M. Hashimoto, B. J. Wiley, D. Ham and G. M. Whitesides, *Adv. Mater.*, 2010, **22**, 2749–2752.
5 S. H. Jeong, A. Hagman, K. Hjort, M. Jobs, J. Sundqvist and Z. G. Wu, *Lab Chip*, 2012, **12**, 4657–4664.
6 S. H. Jeong, K. Hjort and Z. G. Wu, *Sensors*, 2014, **14**, 16311–16321.
7 L. Wang and J. Liu, *RSC Adv.*, 2015, **5**, 57686–57691.
8 S. H. Jeong, K. Hjort and Z. G. Wu, *Sci. Rep-Uk.*, 2015, **5**, 08419.
9 Y. Gao, H. Li and J. Liu, *PLoS One*, 2012, **7**, e45458.
10 Y. Zheng, Z. He, Y. Gao and J. Liu, *Sci. Rep-Uk.*, 2013, **3**, 01786.
11 A. Tabatabai, A. Fassler, C. Usiak and C. Majidi, *Langmuir*, 2013, **29**, 6194–6200.
12 C. Ladd, J. So, J. Muth and M. D. Dickey, *Adv. Mater.*, 2013, **25**, 5081–5085.
13 J. W. Boley, E. L. White, G. T.-C. Chiu and R. K. Kramer, *Adv. Funct. Mater.*, 2014, **24**, 3501–3507.
14 Y. Zheng, Z. Z. He, J. Yang and J. Liu, *Sci. Rep-Uk.*, 2014, **4**, 04588.
15 Q. Zhang, Y. Gao and J. Liu, *Appl. Phys. A: Mater. Sci. Process.*, 2014, **116**, 1091–1097.
16 L. Wang and J. Liu, *RSC Adv.*, 2015, **5**, 57686–57691.
17 S. Cheng and Z. G. Wu, *Lab Chip*, 2010, **10**, 3227–3234.
18 C. Fassler and C. Majidi, *Smart Mater. Struct.*, 2013, **22**, 055023.
19 E. Palleau, S. Reece, S. C. Desai, M. E. Smith and M. D. Dickey, *Adv. Mater.*, 2013, **25**, 1589–1592.
20 H.-J. Kim, C. Son and B. Ziaie, *Appl. Phys. Lett.*, 2008, **92**, 011904.
21 S. Zhu, J.-H. So, R. Mays, S. Desai, W. R. Barnes, B. Pourdeyhimi and M. D. Dickey, *Adv. Funct. Mater.*, 2013, **23**, 2308–2314.
22 R. K. Kramer, C. Majidi and R. J. Wood, *Adv. Funct. Mater.*, 2013, **23**, 5292–5296.
23 G. Li, X. Wu and D.-W. Lee, *Sens. Actuators, B*, 2015, **221**, 1114–1119.
24 G. Li, X. Wu and D.-W. Lee, *2015 Transducers - 2015 18th International Conference on 2015, Solid-State Sensors, Actuators and Microsystems (TRANSDUCERS)*, pp. 339–342.
25 I. D. Joshipura, H. R. Ayers, C. Majidi and M. D. Dickey, *J. Mater. Chem. C*, 2015, **3**, 3834–3841.
26 J. W. Boley, E. L. White and R. K. Kramer, *Adv. Mater.*, 2015, **27**, 2355–2360.
27 G. Li, M. Parmar, D. Kim, J.-B. Lee and D.-W. Lee, *Lab Chip*, 2014, **14**, 200–209.
28 G. Li, M. Parmar and D.-W. Lee, *Nanotechnology (IEEE-NANO), 2013 13th IEEE Conference on 2013*, pp. 410–413.
29 G. Li, M. Parmar and D.-W. Lee, *Lab Chip*, 2015, **15**, 766–775.
30 M. D. Dickey, R. C. Chiechi, R. J. Larsen, E. A. Weiss, D. A. Weitz and G. M. Whitesides, *Adv. Funct. Mater.*, 2008, **18**, 1097–1104.

 This journal is © The Royal Society of Chemistry 2016

31 Q. Xu, N. Oudalov, Q. Guo, H. M. Jaeger and E. Brown, *Phys. Fluids*, 2012, **24**, 063101.
32 R. J. Larsen, M. D. Dickey, G. M. Whitesides and D. A. Weitz, *J. Rheol.*, 2009, **53**, 1305.
33 S. Tang, Y. Lin, I. D. Joshipura, K. Khoshmanesh and M. D. Dickey, *Lab Chip*, 2015, **15**, 3905–3911.
34 M. P. Brenner, J. Eggers, K. Joseph, S. R. Nagel and X. D. Shi, *Phys. Fluids*, 1997, **9**, 1573–1590.
35 B. Ambravaneswaran, S. D. Phillips and O. A. Basaran, *Phys. Rev. Lett.*, 2000, **85**, 5332–5335.
36 B. Ambravaneswaran, H. J. Subramani, S. D. Phillips and O. A. Basaran, *Phys. Rev. Lett.*, 2004, **93**, 034501.
37 P. Coullet, L. Mahadevan and C. S. Riera, *J. Fluid Mech.*, 2005, **526**, 1–17.
38 S. P. Lin and R. D. Reitz, *Annu. Rev. Fluid Mech.*, 1998, **30**, 85–105.
39 L. Rayleigh, *Proc. London Math. Soc.*, 1878, **s1–10**, 4–13.
40 W. V. Hoeve, S. Gekle, J. H. Snoeijer, M. Versluis, M. P. Brenner and D. Lohse, *Phys. Fluids*, 2010, **22**, 122003.
41 D. Kim, J. H. Yoo, Y. Lee, W. Choi, K. Yoo and J.-B. Lee, *Micro Electro Mechanical Systems (MEMS), 2014 IEEE 27th International Conference on 2014*, pp. 967–970.
42 J. Thelen, M. D. Dickey and T. Ward, *Lab Chip*, 2012, **12**, 3961–3967.
43 T. Hutter, W. C. Bauer, S. R. Elliott and W. T. S. Huck, *Adv. Funct. Mater.*, 2012, **22**, 2624–2631.
44 M. D. Dickey, *ACS Appl. Mater. Interfaces*, 2014, **6**, 18369–18379.
45 B. Gol, F. J. Tovar-Lopez, M. E. Kurdzinski, S. Tang, P. Petersen, A. Mitchell and K. Khoshmanesha, *Lab Chip*, 2015, **15**, 2476–2485.
46 J. H. So, J. Thelen, A. Qusba, G. J. Hayes, G. Lazzi and M. D. Dickey, *Adv. Funct. Mater.*, 2009, **19**, 3632–3637.

This journal is © The Royal Society of Chemistry 2016